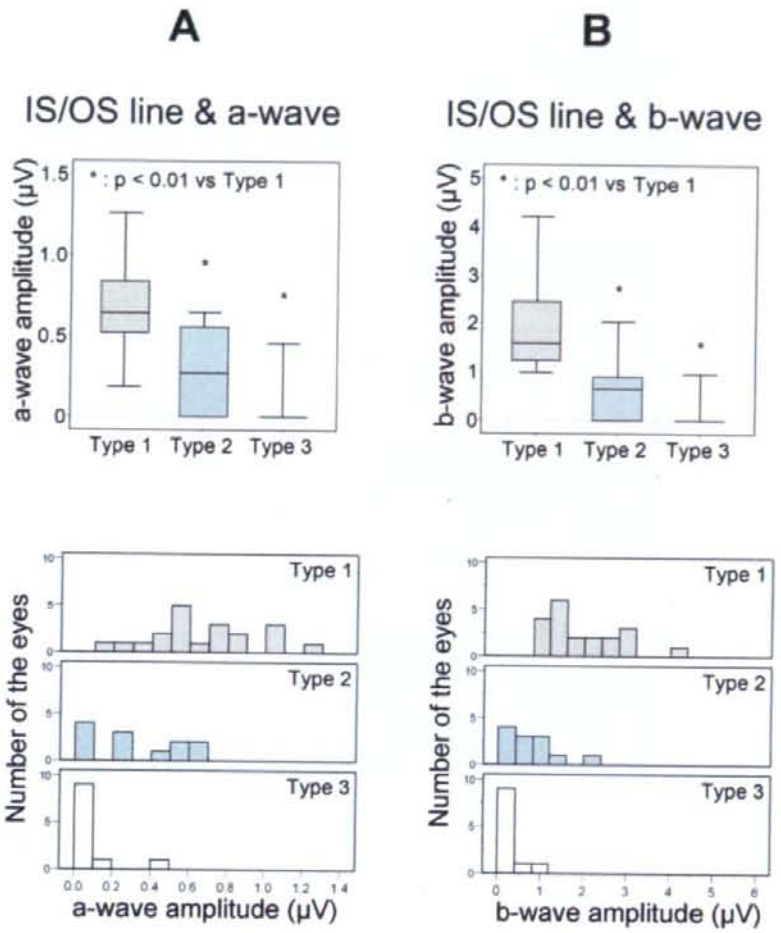

FIGURE 5. The (A) a- and (B) b-wave amplitudes of the fmERGs for patients with RP with the three types of IS/OS line configuration (see also Fig. 1). *Top*: The fmERG amplitudes in type 1 patients with RP were significantly larger than those in type 2 or 3 patients with RP. *Bottom*: histograms of the fmERG amplitude for three types of patients with RP.

in Figure 6. Against our expectations, the length of IS/OS line was relatively well-preserved (>4 mm) for these four patients, and was more than 5 mm for three patients (patients 4, 5, and 7). These results indicated that there are some patients with RP whose total macular volume and the length of IS/OS line were relatively well preserved in the macular area, but their electrophysiological function within this area was severely affected.

DISCUSSION

Our results demonstrated that there was a significant correlation between the amplitudes of the a- and b-waves of the fmERG and the total macular volume in our 43 patients with RP. These results were not surprising because the gradual thinning of the retina caused by the shortening of outer segments and the loss of photoreceptors should result in the reduction of the fmERG amplitude in the retina of patients with RP. The results of an earlier study on the correlation between the retinal histopathology and ERG findings in an animal model of RP support this idea.[52]

Although there was a significant correlation between the amplitude of the fmERG and total macular volume, the degree of correlation was weak: the coefficient of correlation (ρ) was only 0.46 for the a-wave, and 0.54 for the b-wave. One of the major reasons for this weak correlation was that there were four patients with RP who had normal macular volume but severely reduced fmERG amplitudes (Fig. 4). In contrast, there were no patients with RP who had normal fmERG amplitude but severely reduced total macular volume. These results indicate that a normal total macular volume does not guarantee normal electrophysiological function of the macula in patients with RP.

We initially reasoned that the weak correlation might be because we used total macular volume as a measure of macular structure. It is well known that the early histopathologic changes in eyes of patients with RP were mainly a shortening or distortion of the rod and cone photoreceptors.[6–8] Thus, we next investigated whether the structural integrity of the IS/OS junction (i.e., the length of the IS/OS line) correlated with the amplitude of the fmERG. As shown, the length of the IS/OS line generally correlated with the fmERG amplitude. However, the correlation between the length of IS/OS line and the fmERG amplitude was also weak. Careful examinations of the OCT images and fmERG records in individual patients with RP

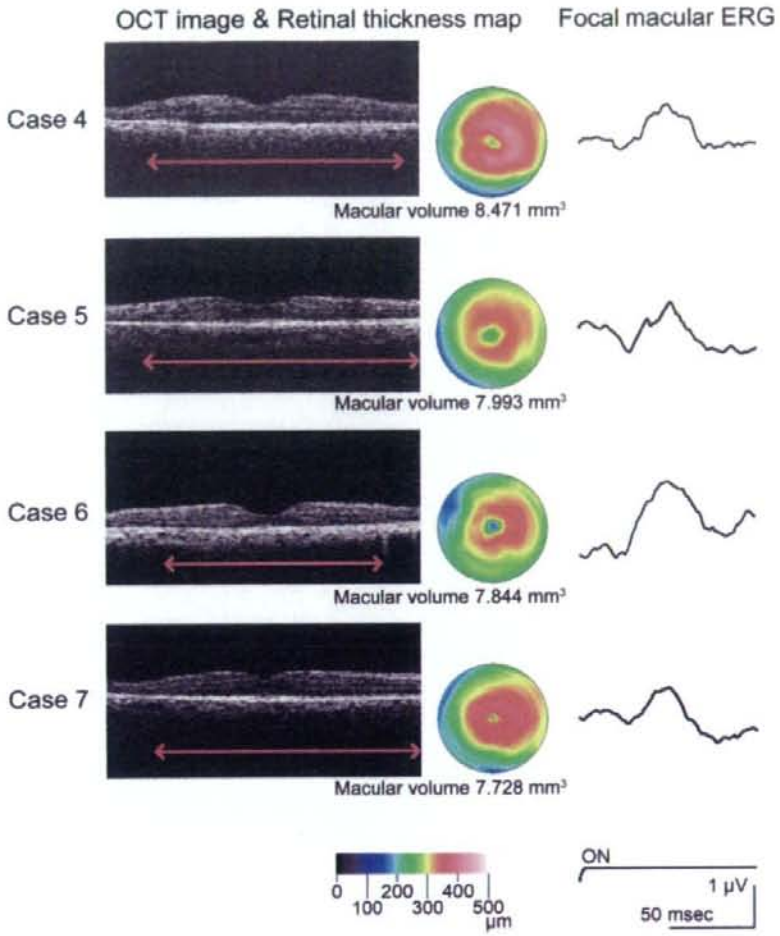

FIGURE 6. Gray-scale OCT images and fmERGs recorded in four patients with RP who had normal macular volume but severely reduced fmERG (see also Fig. 4). *Red lines*: the length of detectable IS/OS lines on the gray-scale OCT images. The amplitudes of fmERGs were severely reduced in all four patients, but the length of the IS/OS line was more than 4 mm in all patients and was more than 5 mm in three of five patients.

showed that there were four patients with RP who had normal macular volume and a relatively long IS/OS line, but severely reduced fmERG amplitudes (Fig. 6). Of interest, three of these four patients had a detectable IS/OS line longer than 5 mm. These results indicated that there are some patients with RP whose macular OCT images are relatively well preserved, but their electrophysiological functions are severely reduced.

The exact reason that some patients with RP had a preserved macular OCT image but severely reduced fmERG was not determined. There are two possibilities: First, these patients may have very subtle structural changes, but our OCT system (third-generation Stratus OCT) may not have detected the changes. For example, using ultrahigh-resolution OCT, Witkin et al.[30] measured the distance between the IS/OS line and the outer border of the retinal pigment epithelium thickness (called FOSPET), and demonstrated an excellent correlation between visual acuity and FOSPET in nine patients with RP. In our study, we were able to measure the length of the IS/OS line, but could not obtain reliable measurements of FOSPET in our OCT images. New-generation, high-resolution OCT instruments may enable us to make these measurements.

A second possibility is that the functional abnormality may precede structural changes in the macula of some patients with RP. It was recently demonstrated that some patients with Leber congenital amaurosis (LCA), the most common inherited cause of blindness in childhood, can retain the cone photoreceptors and inner retinal architecture in the central retina, but have severely reduced central vision at a relatively early stage of the disease.[29,31] If this second possibility is correct, the combined assessment of macular structure by OCT and macular function by psychophysics or electrophysiology can provide important information on the macula of patients with RP.

There are some limitations in our study. First, we planned to measure the volume of the inner, middle, and outer retinal layers separately and wanted to examine the correlation between the volumes in each layer and the fmERG amplitude. This comparison was possible in normal subjects, but was difficult in patients with RP with severely reduced macular thickness. Recent advances in new ultrahigh-resolution OCT technique may enable analysis of the thickness of each retinal layer, and this will allow us to investigate the changes in each retinal layer after photoreceptor degenerations. Second, we investigated the correlation of macular volume with the fmERG amplitude, but did not study the correlation with the implicit time, because there were many patients with RP whose amplitude of fmERG was so reduced that the implicit time could not

be measured precisely. However, the correlation between the implicit time and OCT images may be interesting, because the results of past studies have shown that the delay in the implicit time of focal ERGs can be another important indicator of functional changes in the macula area of patients with RP.[14-19] Third, we did not record the OCT and mfERGs from the same patient at different time points, and thus cannot examine the longitudinal progression of the changes in patients with RP.

In conclusion, we studied the correlation between the fmERG amplitude and macular structure by OCT and found that there was a significant correlation between these two measures, but the degree of correlation was weak. One major reason for this low correlation was the presence of some patients with RP who had well-preserved macular OCT images but severely reduced fmERGs. Although the exact mechanism for this discrepancy needs further investigation, we believe that the combined examination of macular structure by OCT and macular function by fmERG can provide important information on the pathophysiology, prognosis, and future treatments in patients with RP.

References

1. Carr RE, Heckenlively JR. Hereditary pigmentary degenerations of the retina. In: Duane TD, Jaeger EA, eds. *Clinical Ophthalmology*. Philadelphia: JB Lippincott; 1987;1-28.
2. Heckenlively JR. RP syndromes. In: Heckenlively JR, ed. *Retinitis Pigmentosa*. Philadelphia: JB Lippincott; 1988;221-252.
3. Newsome DA. Retinitis pigmentosa, Usher's syndrome, and other pigmentary retinopathies. In: Newsome DA, ed. *Retinal Dystrophies and Degenerations*. New York: Raven Press; 1988;161-194.
4. Weleber RG, Gregory-Evance K. Retinitis pigmentosa and allied disorders. In: Hinton DR, ed. *Retina*. 4th ed. Vol. 1. Basic science and inherited retinal disease. St. Louis: Mosby; 2006;395-498.
5. Hartong DT, Berson EL, Dryja TP. Retinitis pigmentosa. *Lancet*. 2006;368:1795-1809.
6. Szamier RB, Berson EL, Klein R, Meyers S. Sex-linked retinitis pigmentosa: ultrastructure of photoreceptors and pigment epithelium. *Invest Ophthalmol Vis Sci*. 1979;18:145-160.
7. Milam AH, Li ZY, Fariss RN. Histopathology of the human retina in retinitis pigmentosa. *Prog Retin Eye Res*. 1998;175-205.
8. Fariss RN, Li ZY, Milam AH. Abnormalities in rod photoreceptors, amacrine cells, and horizontal cells in human retinas with retinitis pigmentosa. *Am J Ophthalmol*. 2000;129:215-223.
9. Sandberg MA, Effron MH, Berson EL. Focal cone electroretinograms in dominant retinitis pigmentosa with reduced penetrance. *Invest Ophthalmol Vis Sci*. 1978;17:1096-1101.
10. Biersdorf WR. Temporal factors in the foveal ERG. *Curr Eye Res*. 1982;1:717-722.
11. Seiple W, Siegel IM, Carr RE, Mayron C. Evaluating macular function using the focal ERG. *Invest Ophthalmol Vis Sci*. 1986;27:1123-1130.
12. Falsini B, Iarossi G, Porciatti V, et al. Postreceptoral contribution to macular dysfunction in retinitis pigmentosa. *Invest Ophthalmol Vis Sci*. 1994;35:4282-4290.
13. Ikenoya K, Kondo M, Piao CH, et al. Preservation of macular oscillatory potentials in eyes of patients with retinitis pigmentosa and normal visual acuity. *Invest Ophthalmol Vis Sci*. 2007;48:3312-3317.
14. Hood DC, Holopigian K, Greenstein V, et al. Assessment of local retinal function in patients with retinitis pigmentosa using the multi-focal ERG technique. *Vision Res*. 1998;38:163-179.
15. Chan HL, Brown B. Investigation of retinitis pigmentosa using the multifocal electroretinogram. *Ophthalmic Physiol Opt*. 1998;18:335-350.
16. Seeliger MW, Kretschmann UH, Apfelstedt-Sylla E, Zrenner E. Implicit time topography of multifocal electroretinograms. *Invest Ophthalmol Vis Sci*. 1998;39:718-723.
17. Felius J, Swanson WH. Photopic temporal processing in retinitis pigmentosa. *Invest Ophthalmol Vis Sci*. 1999;40:2932-2944.
18. Hood DC. Assessing retinal function with the multifocal technique. *Prog Retin Eye Res*. 2000;19:607-646.
19. Holopigian K, Seiple W, Greenstein VC, et al. Local cone and rod system function in patients with retinitis pigmentosa. *Invest Ophthalmol Vis Sci*. 2001;42:779-788.
20. Vajaranant TS, Seiple W, Szlyk JP, Fishman GA. Detection using the multifocal electroretinogram of mosaic retinal dysfunction in carriers of X-linked retinitis pigmentosa. *Ophthalmology*. 2002;109:560-568.
21. Robson AG, Saihan Z, Jenkins SA, et al. Functional characterization and serial imaging of abnormal fundus autofluorescence in patients with retinitis pigmentosa and normal visual acuity. *Br J Ophthalmol*. 2006;90:472-479.
22. Jacobson SG, Buraczynska M, Milam AH, et al. Disease expression in X-linked retinitis pigmentosa caused by a putative null mutation in the RPGR gene. *Invest Ophthalmol Vis Sci*. 1997;38:1983-1997.
23. Jacobson SG, Cideciyan AV, Huang Y, et al. Retinal degenerations with truncation mutations in the cone-rod homeobox (CRX) gene. *Invest Ophthalmol Vis Sci*. 1998;39:2417-2426.
24. Jacobson SG, Cideciyan AV, Iannaccone A, et al. Disease expression of RP1 mutations causing autosomal dominant retinitis pigmentosa. *Invest Ophthalmol Vis Sci*. 2000;41:1898-1908.
25. Schatz P, Abrahamson M, Eksandh L, Ponjavic V, Andréasson S. Macular appearance by means of OCT and electrophysiology in members of two families with different mutations in RDS (the peripherin/RDS gene). *Acta Ophthalmol Scand*. 2003;81:500-507.
26. Jacobson SG, Cideciyan AV, Aleman TS, et al. Crumbs homolog 1 (CRB1) mutations result in a thick human retina with abnormal lamination. *Hum Mol Genet*. 2003;12:1073-1078.
27. Sandberg MA, Brockhurst RJ, Gaudio AR, Berson EL. The association between visual acuity and central retinal thickness in retinitis pigmentosa. *Invest Ophthalmol Vis Sci*. 2005;46:3349-3354.
28. Schwartz SB, Aleman TS, Cideciyan AV, et al. Disease expression in Usher syndrome caused by VLGR1 gene mutation (USH2C) and comparison with USH2A phenotype. *Invest Ophthalmol Vis Sci*. 2005;46:734-743.
29. Jacobson SG, Aleman TS, Cideciyan AV, et al. Identifying photoreceptors in blind eyes caused by RPE65 mutations: prerequisite for human gene therapy success. *Proc Natl Acad Sci USA*. 2006;102:6177-6182.
30. Witkin AJ, Ko TH, Fujimoto JG, et al. Ultra-high resolution optical coherence tomography assessment of photoreceptors in retinitis pigmentosa and related diseases. *Am J Ophthalmol*. 2006;142:945-952.
31. Cideciyan AV, Aleman TS, Jacobson SG, et al. Centrosomal-ciliary gene CEP290/NPHP6 mutations result in blindness with unexpected sparing of photoreceptors and visual brain: implications for therapy of Leber congenital amaurosis. *Hum Mutat*. 2007;28:1074-1083.
32. Jacobson SG, Cideciyan AV, Aleman TS, et al. Leber congenital amaurosis caused by an RPGRIP1 mutation shows treatment potential. *Ophthalmology*. 2007;114:895-898.
33. Aleman TS, Cideciyan AV, Sumaroka A, et al. Inner retinal abnormalities in X-linked retinitis pigmentosa with RPGR mutations. *Invest Ophthalmol Vis Sci*. 2007;48:4759-4765.
34. Apushkin MA, Fishman GA, Alexander KR, Shahidi M. Retinal thickness and visual thresholds measured in patients with retinitis pigmentosa. *Retina*. 2007;27:349-357.
35. Walia S, Fishman GA, Edward DP, Lindeman M. Retinal nerve fiber layer defects in RP patients. *Invest Ophthalmol Vis Sci*. 2007;8:4748-4752.
36. Matsuo T, Morimoto N. Visual acuity and perimacular retinal layers detected by optical coherence tomography in patients with retinitis pigmentosa. *Br J Ophthalmol*. 2007;91:888-9033.
37. Horio N, Kachi S, Hori K, et al. Progressive change of optical coherence tomography scans in retinal degeneration slow mice. *Arch Ophthalmol*. 2001;119:1329-1332.
38. Li Q, Timmers AM, Hunter K, et al. Noninvasive imaging by optical coherence tomography to monitor retinal degeneration in the mouse. *Invest Ophthalmol Vis Sci*. 2001;42:2981-2989.

39. Huang Y, Cideciyan AV, Papastergiou GI, et al. Relation of optical coherence tomography to microanatomy in normal and rd chickens. *Invest Ophthalmol Vis Sci*. 1998;39:2405–2416.
40. Huang Y, Cideciyan AV, Alemán TS, et al. Optical coherence tomography (OCT) abnormalities in rhodopsin mutant transgenic swine with retinal degeneration. *Exp Eye Res*. 2000;70:247–251.
41. Marmor MF, Holder GE, Seeliger MW, Yamamoto S; International Society for Clinical Electrophysiology of Vision. Standard for clinical electroretinography (2004 update). *Doc Ophthalmol*. 2004; 108:107–114.
42. Miyake Y, Shiroyama N, Ota I, Horiguchi M. Oscillatory potentials in electroretinograms of the human macular region. *Invest Ophthalmol Vis Sci*. 1988;29:1631–1635.
43. Miyake Y. Studies of local macular ERG (in Japanese). *Acta Soc Ophthalmol Jpn*. 1988;92:1418–1449.
44. Wong TY, Foster PJ, Ng TP, et al. Variations in ocular biometry in an adult Chinese population in Singapore: the Tanjong Pagar Survey. *Invest Ophthalmol Vis Sci*. 2001;42:73–80.
45. Shufelt C, Fraser-Bell S, Ying-Lai M, et al. Refractive error, ocular biometry, and lens opalescence in an adult population: the Los Angeles Latino Eye Study. *Invest Ophthalmol Vis Sci*. 2005;46: 4450–4460.
46. Olsen T, Arnarsson A, Sasaki H, et al. On the ocular refractive components: the Reykjavik Eye Study. *Acta Ophthalmol Scand*. 2007;85:361–366.
47. Costa RA, Calucci D, Skaf M, et al. Optical coherence tomography 3: Automatic delineation of the outer neural retinal boundary and its influence on retinal thickness measurements. *Invest Ophthalmol Vis Sci*. 2004;45:2399–2406.
48. Ishikawa K, Kondo M, Ito Y, et al. Correlation between focal macular electroretinograms and angiographic findings after photodynamic therapy. *Invest Ophthalmol Vis Sci*. 2007;48:2254–2259.
49. Drexler W, Sattmann H, Hermann B, et al. Enhanced visualization of macular pathology with the use of ultrahigh-resolution optical coherence tomography. *Arch Ophthalmol*. 2003;121:695–706.
50. Costa RA, Skaf M, Melo LA Jr, et al. Retinal assessment using optical coherence tomography. *Prog Retin Eye Res*. 2006;25:325–353.
51. Pons ME, and Garcia-Valenzuela E. Redefining the limit of the outer retina in optical coherence tomography scans. *Ophthalmology*. 2005;112:1079–1085.
52. Machida S, Kondo M, Jamison JA, et al. P23H rhodopsin transgenic rat: correlation of retinal function with histopathology. *Invest Ophthalmol Vis Sci*. 2000;41:3200–3209.

Japanese Journal of Applied Physics
Vol. 47, No. 4, 2008, pp. 3220–3225

©2008 The Japan Society of Applied Physics

Retinal Stimulation on Rabbit Using Complementary Metal Oxide Semiconductor Based Multichip Flexible Stimulator toward Retinal Prosthesis

Takashi TOKUDA, Ryosuke ASANO, Sachie SUGITANI, Mari TANIYAMA, Yasuo TERASAWA[1], Masahiro NUNOSHITA, Kazuaki NAKAUCHI[2], Takashi FUJIKADO[2], Yasuo TANO[2], and Jun OHTA

Graduate School of Materials Science, Nara Institute of Science and Technology, 8916-5 Takayama, Ikoma, Nara 630-0192, Japan
[1]*Vision Institute, NIDEK Co., Ltd., 73-1 Hama, Gamagori, Aichi 443-0036, Japan*
[2]*Department of Ophthalmology, Osaka University Medical School, 2-15 Yamadaoka, Suita, Osaka 565-0871, Japan*

(Received October 2, 2007; accepted December 10, 2007; published online April 25, 2008)

The Functionality of a complementary metal oxide semiconductor (CMOS) LSI-based, multichip flexible retinal stimulator was demonstrated in retinal stimulation experiments on rabbits. A 1 × 4-configured multichip stimulator was fabricated for application to experiments on animals. An experimental procedure including surgical operations was developed, and retinal stimulation was performed with the fabricated multichip stimulator. Neural responses on the visual cortex were successfully evoked by the fabricated stimulator. The stimulator is confirmed to be applicable to acute animal experiments.
[DOI: 10.1143/JJAP.47.3220]

KEYWORDS: retinal prosthesis, CMOS stimulator, multichip architecture

1. Introduction

LSI-based neural interfacing/rehabilitation/prosthesis technology is one of the research fields in which electronics technology can provide new and powerful solutions.[1–4] Retinal prosthesis technology is a biomedical application for which LSI-based devices can play an essential role.[5–16] For cases of retinitis pigmentosa (RP) and age-related macular degeneration (AMD), it is reported that only photoreceptor cells are impaired and other neural layers partially remain. Retinal prosthesis is a neural prosthesis technology that aims to provide a substitutional visual sensation with patterned electric stimulation of the visual nerve system. A number of projects developing retinal prosthesis systems using different technical approaches are now under way in Japan, the United States, Germany, and other countries.[5–16]

Compared with an electrode array fabricated on a flexible substrate with printed patterns, the LSI-based stimulator is a powerful platform for high-resolution retinal stimulation. To realize a flexible LSI-based retinal stimulator, we proposed to configure a flexible retinal stimulator with an array of small LSI stimulators (unit chip) that can be operated cooperatively. We have reported on the design, packaging, and functional characterization of a multichip retinal stimulator.[13–16]

In this work, we designed a new unit chip and assembled it into a flexible stimulator for retinal stimulation of a rabbit's eye. We developed an experimental procedure including surgical implant operations, and performed retinal stimulation of an anesthetized rabbit's eye. Many works have been reported on *in vivo* retinal stimulation for application to retinal prosthesis.[10–12] However, *in vivo* retinal stimulation using an LSI-based stimulator has been hardly reported. We describe in detail the retinal stimulation of a rabbit's retina, and present the results obtained showing the functionality of the fabricated multichip flexible retinal stimulator.

2. Fabrication of Multichip Flexible Stimulator for Animal Experiments

Figure 1 shows the concept of a multichip flexible retinal stimulator. A small multielectrode complementary metal oxide semiconductor (CMOS) stimulator, "unit chip", is mounted on a flexible substrate with appropriate spacing. With this structure, the stimulator can be bent between unit chips. Currently, each unit chip is a single-site stimulator with addressable stimulation electrodes.

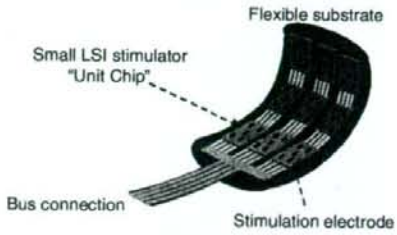

Fig. 1. Concept of multichip flexible retinal stimulator.

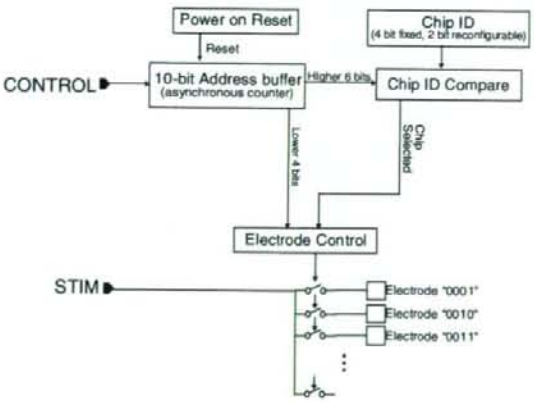

Fig. 2. Block diagram of unit chip.

Figure 2 shows a block diagram of the unit chip. The unit chip has nine stimulation output pads and four control inputs: VDD, GND, CONTROL, and STIM. The VDD and GND lines are used for continuous power supply, and the operation voltage of the unit chip is DC 5 V. The CONTROL

Table I. Specifications of unit chips designed in present and previous studies.

	Present (Third generation)	Previous[15,16] (Second generation)	Previous[13,14] (First generation)
Fabrication process	0.35 μm 2-poly 4-metal standard CMOS	0.35 μm 2-poly 4-metal standard CMOS	0.6 μm 2-poly 3-metal standard CMOS
Unit chip size (μm^2)	600 × 600	600 × 600	600 × 600
Series resistance (Ω)	~200	~200	$\sim 1 \times 10^3$
Reset sequence	Power on reset	Power on reset	Logic
Number of electrodes per unit chip	9	9	9
Address space for unit chip (bit)	6	6	4
(Maximum number of unit chips)	(64)	(64)	(16)
Maximum number of electrodes in multichip stimulator	576	576	144
Number of reconfigurable bits in chip ID (bit)	2/6	6/6	0/4

line is used for addressing. The unit chip has a 10-bit asynchronous counter for the address buffer. It counts the number of digital pulses applied on the CONTROL input and interprets it as the address of the stimulation electrode. The STIM line is used for stimulation. After the control pulses are applied on the CONTROL line, the STIM input is connected to the selected stimulation electrode via a transmission-gate switch. The lower 4 bits in the address buffer are used for the selection of stimulation electrodes. The stimulation electrodes on the unit chip have 4-bit addresses from "0000" to "1001". The upper 6 bits are used to choose one of the unit chips assembled on the flexible stimulator. Each unit chip has a 6-bit unique ID for identification. The connection between the STIM input and the selected electrode is enabled on the unit chip whose ID matches with the upper 6 bits in the address buffer. Therefore, any stimulation electrode on the multichip flexible stimulator can be selected with the number of digital pulses applied on the CONTROL input. In the current architecture, in the maximum configuration, we can realize a multichip stimulator that has 64 unit chips and 576 stimulation electrodes.

Figure 3 shows the layout of the unit chip designed in the present work. The current unit chip is the third generation in our continuous development of the multichip flexible stimulator.[13–16] Table I shows the specifications of the current and previous unit chips. The current unit chip was fabricated by a 0.35 μm 2-poly, 4-metal standard CMOS process using a high-voltage (5 V) option. The basic functionality and specifications of the present unit chip (third generation) are the same as those of the chip in the second generation, and their detailed description was presented in our previous reports.[15,16] As the only revised feature, the number of reconfigurable bits in the chip ID is reduced from 6 to 2. Thus, only the upper 2 bits of the 6-bit chip ID can be modified by fuse amputation. This is reasonable because we designed an LSI die on which 16 unit chips with chip IDs from "000000" to "001111" are aligned, and we can cover all chip IDs reconfiguring the highest 2 bits in the chip ID. The series resistance shown in Table I is an ON resistance of the CMOS switch (transmission gate) that establishes a connection between the STIM input and the selected electrode. The CMOS switch consists of a

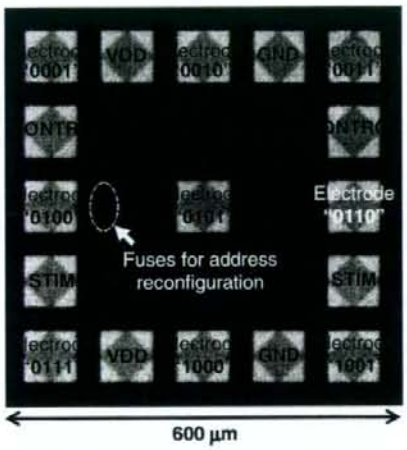

Fig. 3. Layout of unit chip.

parallel set of NMOS and PMOS transistors. In the first generation, the series resistance is as large as 1 kΩ, but it is reduced to a value less than 200 Ω in the unit chip in the second generation.[16] In the present design (the third generation), the CMOS switch circuitry is basically identical with that in the second generation.

Packaging is another essential issue using in the case of the CMOS-based device for bioimplant applications. The CMOS device must be molded in a waterproof and biocompatible material. In the present work, we aimed to realize a multichip stimulator durable for acute (less than several hours) animal experiments. We assembled a multichip flexible stimulator with the structure developed in the previous work.[16] Figure 4 shows the structure of the presentmultichip stimulator. The detailed packaging process for the device structure shown in Fig. 4 is described in ref. 16.

In this work, we chose a configuration with a 1 × 4 unit chip array, which matched the size of a rabbit's eye. Figure 5 show photographs of the multichip stimulator fabricated for functional demonstration in animal experiments using rabbits. As shown in Fig. 5, the device can be bent with a radius of curvature $r = 1.7$ mm, and the device can be fit on

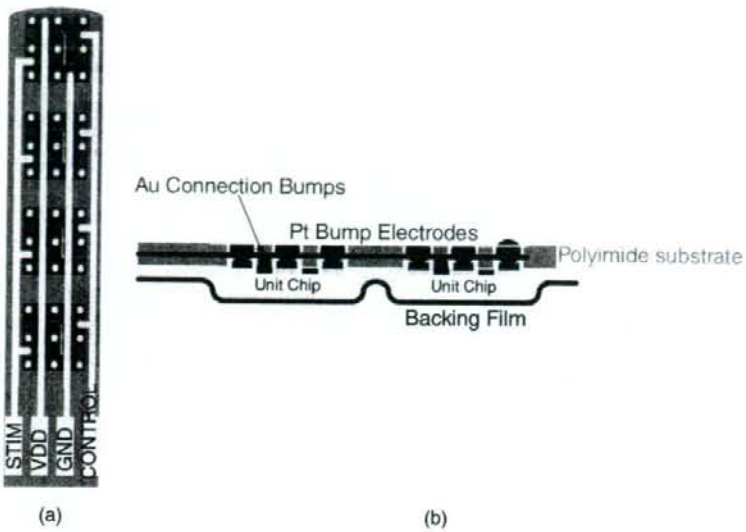

Fig. 4. Structure of multichip retinal stimulator: (a) plan view and (b) cross section.

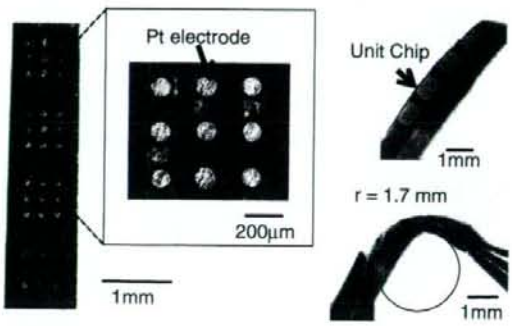

Fig. 5. Multichip flexible retinal stimulator for retinal stimulation experiments on rabbits.

a rabbit's eye. The diameter of the bulk Pt stimulation electrode is typically 90 μm, and the pitches of the stimulation electrodes are 240 (within the unit-chip) and 620 (between two adjacent unit chips) μm.

3. Stimulation Experiments on Rabbit's Retina Using the Multichip Flexible Stimulator

3.1 Experimental procedure

To demonstrate and characterize the functionality of the multichip flexible stimulator, we performed retinal stimulation experiments using rabbits. We confirmed that the fabricated multichip flexible stimulator can be surgically implanted in a rabbit's eye, and used for the stimulation of the retina. Response in the visual cortex of the brain was also recorded. Figure 6 schematically shows the configuration of the experiments on rabbits. Electrically evoked potential (EEP) measurement was performed by stimulating the retina with the present multichip stimulator [Fig. 6(a)]. Figure 6(b) shows the configuration of screw electrodes in the visual

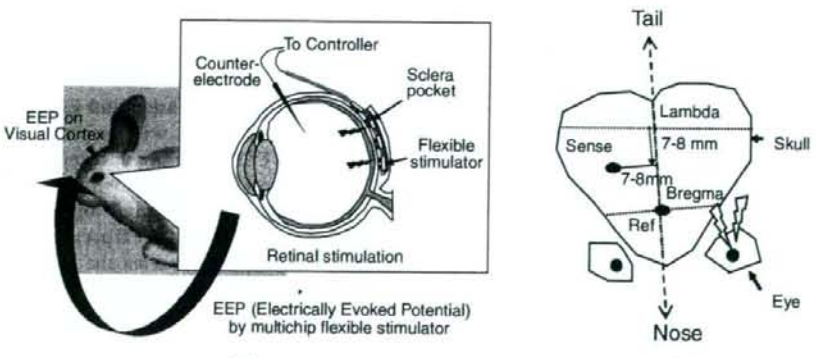

Fig. 6. (a) Experimental configuration and (b) positions of screw electrodes on skull for measurement.

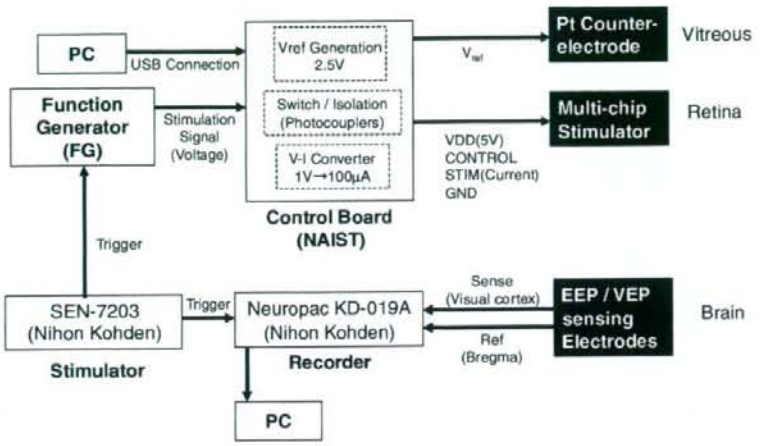

Fig. 7. Measurement setup for EEP/VEP measurement.

cortex for measurement. All the experiments were carried out following the Institutional Guidelines of Osaka University and the ARVO Resolution on the Use of Animals in Ophthalmic Research.

A non-SPF (specific-pathogen-free) Dutch belted rabbit with normal sight was used for the animal experiments. The experiments were carried out in a non-SPF part of an animal experimental facility. The experimental procedure was as follows.

Step 1. Anesthesia: The rabbit was anesthetized with an intramuscular injection of ketamine hydrochloride (50 mg/kg) and xylazine hydrochloride (5 mg/kg), which provides stable anesthesia for more than 2 h. Additional injections were also carried out to control appropriate anesthesia depth.

Step 2. Implantation of screw electrodes for measurement: Stainless-steel screw electrodes were implanted into the visual cortex through the skull to measure the response to retinal stimulation. The position of the sensing electrode is shown in Fig. 6(b). And the reference electrode was implanted into the bregma.

Step 3. Implantation of multichip flexible stimulator: A 1×4-configured multichip retinal stimulator was implanted and fixed in a suprachoroidal transretinal stimulation (STS) configuration. STS is a retinal stimulation scheme proposed by a group in Osaka University.[17,18] The retinal stimulator is placed outside the vitreous (behind the retina), and a counter-electrode is placed in the vitreous. Stimulation current injection is performed through the retina and choroid. In the present work, the stimulator was inserted in a scleral pocket formed by partial incision [see, Fig. 6(a)]. The position and size of the scleral pocket were approximately 12 mm from limbs, and typically 2.0 mm in width and 4.0 mm in length. The top of the stimulator head was positioned near the visual streak of the eye.

Step 4. Implantation of Pt counterelectrode in vitreous: A polyurethane-coated wire Pt counterelectrode was inserted into the vitreous. The coating layer at the end of the wire was removed, and the Pt counterelectrode was exposed. The Pt counterelectrode was inserted into the sclera. The distance between the insertion point and the limbus was approximately 1 mm.

Step 5. Connection of the stimulator and electrodes to measurement system: After all the surgical operations were completed under deeply anesthetized condition, the rabbit was moved to the measurement bench. The measurement configuration is shown in Fig. 7. The measurement system consisted of a control system for the multichip retinal stimulator, brain wave measurement system (Nihon Kohden Neuropac KD-019A), and a stimulator (Nihon Kohden SEN-7203) for generate a trigger signal for stimulation.

Step 6. Visually evoked potential (VEP) measurement: Since the ketamine hydrochloride + xylazine hydrochloride anesthesia partially inhibits response in the visual cortex, we started the measurement procedure with a VEP measurement. The retina was stimulated with flushing light and response in the visual cortex was measured. A flush bulb (1.2 J) was placed approximately 15 cm from the cornea. The stimuli were provided at 0.5 Hz, and triggered recording was performed. The response was measured 20–30 times and averaged to suppress random noise in the measurement. By checking the VEP response, we confirmed that the anesthesia depth is at the appropriate level, and the screw electrodes in the brain and measurement system are correctly configured and working.

Step 7. Retinal stimulation and EEP measurement: The retinal stimulation was performed under various conditions. EEP response was recorded in the visual cortex. In the present work, we used current-controlled, monophasic anodic injection for retinal stimulation. A constant current (50–500 μA) was transretinally injected in the direction from the sclera to the vitreous for 500 μs. The stimulation was performed at 0.5 Hz, and the response in the visual cortex was measured 20–30 times on average. All the VEP and EEP experimental trials were performed under environmental room light. Environmental room light may cause a small VEP in the visual cortex. However, we have detected no environ-

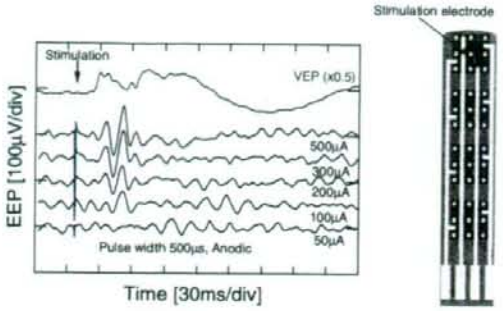

Fig. 8. EEP responses obtained in single-site stimulation trial.

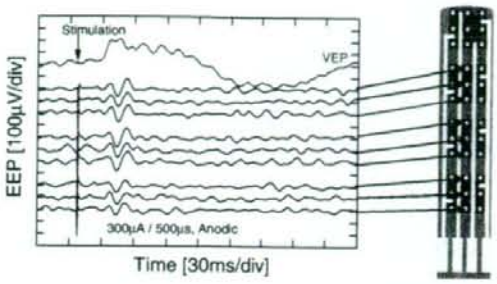

Fig. 9. EEP responses obtained in multichip, multisite stimulation trial.

mental-room-light-induced VEP in the measured VEP and EEP traces, since the brightness of the environmental room light is extremely smaller than that used in VEP measurement.

3.2 *Results*

We performed two kinds of stimulation experiments to demonstrate the functionality of the multichip flexible stimulator. One is a single-site stimulation trial performed with different stimulation strengths, and the other is a multisite, multichip stimulation trial with a constant stimulation strength.

3.2.1 *Single-site stimulation with different stimulation strengths*

To confirm that response in the visual cortex can be evoked under reasonable conditions, we performed single-site stimulation with different stimulation strengths. We fixed the pulse duration at 500 μs, and varied current in the range of 50–500 μA. Figure 8 shows the EEP traces observed in the single-site stimulation. Clear EEP responses were obtained for stimulation currents in the range 100–500 μA. The total charge, charge density, and current density for the threshold condition (100 μA, 500 μs) are 50 nC/pulse, 620 μC/cm^2, and 1.23 A/cm^2. The current/duration and charge for the stimulation are considered to be within typical ranges for the current-controlled retinal stimulation. We can conclude that the present multichip retinal stimulator can be successfully used for experimental applications to retinal prosthesis.

There is a typical difference between the observed VEP and EEP responses. In the VEP traces, peaks tend to fuse. We consider the following reasons for this difference. In the VEP trials, stimulation light excites visual cells in the retina, and neural excitation is transferred to the retinal network layer via synaptic connections. The signal transfer path for VEP includes the response of the visual cells to the stimulation light, and with more synaptic connections the peaks in VEP traces tend to fuse. This mechanism is also supported by the difference in latency, the temporal interval between the stimulation and first the response observed in the brain wave traces. Some EEP traces (for instance, 500 μA stimulation in Fig. 8) have a small peak with a latency of approx. 15 ms, which is smaller than the latency in the VEP traces (19 ms, in Fig. 8).

In the present work, no severe damage was observed in either the rabbit's eyes or the Pt electrodes, owing to the small number of stimulation trials performed in one procedure. However, it should be noted that the waveform (monophasic and charge-unbalanced) and charge density in the present work are inappropriate for chronic retinal stimulation from the viewpoint of safety for both biological tissues and electrode materials.

3.2.2 *Multichip and multisite stimulation with constant strength*

Figure 9 shows the EEP responses obtained in the multichip, multisite stimulation trial. We sequentially performed stimulations using different stimulation electrodes on the center column of the 1 × 4 multichip retinal stimulator (see inset of Fig. 9). Note that the top unit chip was not used in this trial, owing to the error in the packaging process. The pulse conditions were 300 μA/500 μs. As shown in Fig. 9, clear EEP responses were observed in the multichip stimulation trial. Since the stimulator head is not pressed onto the inside of the scleral pocket, a thin electrolyte layer is expected to exist between the stimulation electrodes and the scleral tissue. Furthermore, in the present work, the positions of the multichip stimulator and screw electrodes in the visual cortex are not coordinated each other. This means that a clear positional dependence of the EEP responses should not be expected yet. However, EEP traces in Fig. 9 show a weak dependence on stimulation position. The amplitude observed in the EEP responses corresponding to the electrodes on the unit chip at a large insertion depth was larger than that observed for the other unit chips. This result is quite promising and we can expect application of the multichip stimulator in a two-dimensional stimulation trial. The localization of the visual sensation, which will be one of the essential issue in retinal prosthesis technology, is expected to be demonstrated by EEP measurement with a higher spatial resolution in the visual cortex.

4. Conclusions

A CMOS LSI-based, multichip flexible retinal stimulator was used in stimulation experiments on a rabbit's retina. A 1 × 4-configured multichip stimulator was fabricated for animal experiments. An experimental procedure including surgical operations was developed. Retinal stimulation was performed with the fabricated multichip stimulator, and EEP

responses were successfully observed in the visual cortex of the rabbit's brain. The stimulator is confirmed to be applicable to acute animal experiments. In the future, the development of flexible stimulators with improved durability and biocompatibility for longer experimental applications will be carried out.

Acknowledgements

This work was supported by a Grant for Practical Application of Next-Generation Strategic Technology from the New Energy and Industrial Technology Development Organization (NEDO), Japan, and by Health and Labor Sciences Research Grants from the Ministry of Health, Labour, and Welfare of Japan.

1) K. Najafi and K. D. Wise: IEEE J. Solid-State Circuits **21** (1986) 1035.
2) J. Ji, K. Najafi, and K. D. Wise: IEEE Trans. Biomed. Eng. **38** (1991) 75.
3) T. Kawano, Y. Kato, R. Tani, H. Takao, K. Sawada, and M. Ishida: IEEE Trans. Electron Devices **51** (2004) 415.
4) E. Margalit, J. D. Weiland, R. E. Clatterbuck, G. Y. Fujii, M. Maia, M. Tameesh, G. Torres, S. A. D'Anna, S. Desai, D. V. Piyathaisere, A. Olivi, E. de Juan, and M. S. Humayun: J. Neurosci. Methods **123** (2003) 129.
5) W. Liu, K. Vichienchom, M. Clements, S. C. DeMarco, C. Hughes, E. McGucken, M. S. Humayun, E. de Juan, J. D. Weiland, and R. Greenberg: IEEE J. Solid-State Circuits **35** (2000) 1487.
6) S. C. DeMarco, W. Liu, P. R. Singh, G. Lazzi, M. S. Humayun, and J. D. Weiland: IEEE J. Solid-State Circuits **38** (2003) 1679.
7) D. Palanker, A. Vankov, P. Huie, and S. Baccus: J. Neural Eng. **2** (2005) S105.
8) E. Zrenner, A. Stett, S. Weiss, R. B. Aramant, E. Guenther, K. Kohler, K. D. Miliczek, M. J. Seiler, and H. Haemmerle: Vision Res. **39** (1999) 2555.
9) J. Deguchi, T. Watanabe, T. Nakamura, Y. Nakagawa, T. Fukushima, S. J.-Chill, H. Kurino, T. Abe, M. Tamai, and M. Koyanagi: Jpn. J. Appl. Phys. **43** (2004) 1685.
10) T. Watanabe, R. Kobayashi, K. Komiya, T. Fukushima, H. Tomita, E. Sugano, H. Kurino, T. Tanaka, M. Tamai, and M. Koyanagi: Jpn. J. Appl. Phys. **46** (2007) 2785.
11) D. Güven, J. D. Weiland, G. Fujii, B. V. Mech, M. Mahadevappa, R. Greenberg, R. Roizenblatt, G. Qiu, L. LaBree, X. Wang, D. Hinton, and M. S. Humayun: J. Neural Eng. **2** (2005) S65.
12) J. F. Rizzo III, J. Wyatt, J. Loewenstein, S. Kelly, and D. Shire: Invest. Ophthalmol. Vis. Sci. **44** (2003) 5355.
13) J. Ohta, N. Yoshida, K. Kagawa, and M. Nunoshita: Jpn. J. Appl. Phys. **41** (2002) 2322.
14) T. Tokuda, Y.-L. Pan, A. Uehara, K. Kagawa, M. Nunoshita, and J. Ohta: Sens. Actuators A **122** (2005) 88.
15) J. Ohta, T. Tokuda, K. Kagawa, T. Furumiya, A. Uehara, Y. Terasawa, M. Ozawa, T. Fujikado, and Y. Tano: IEEE Eng. Med. Biol. Mag. **25** (2006) 47.
16) T. Tokuda, S. Sugitani, M. Taniyama, A. Uehara, Y. Terasawa, K. Kagawa, M. Nunoshita, Y. Tano, and J. Ohta: Jpn. J. Appl. Phys. **46** (2007) 2792.
17) H. Kanda, T. Morimoto, T. Fujikado, Y. Tano, Y. Fukuda, and H. Sawai: Invest. Ophthal. Visual Sci. **45** (2004) 560.
18) K. Nakauchi, T. Fujikado, H. Kanda, T. Morimoto, J. S. Choi, Y. Ikuno, H. Sakaguchi, M. Kamei, M. Ohji, T. Yagi, S. Nishimura, H. Sawai, Y. Fukuda, and Y. Tano: Graefes Arch. Clin. Exp. Ophthalmol. **243** (2005) 169.

IEICE Electronics Express, Vol.5, No.15, 574–580

A visual prosthesis with 100 electrodes featuring wireless signals and wireless power transmission

Yasuo Terasawa[1,2a)], Akihiro Uehara[1,2], Eiji Yonezawa[1], Tohru Saitoh[1], Kenzo Shodo[1,2], Motoki Ozawa[1], Yasuo Tano[3], and Jun Ohta[2]

[1] *Vision Institute, Nidek Co.,Ltd*
73–1 Hama-cho, Gamagori, Aichi 443–0036, Japan

[2] *Materials Science, Nara Institute of Science and Technology,*
8916–5 Takayama-cho, Ikoma, Nara 630–0101, Japan

[3] *Department of Ophthalmology, Graduate School of Medicine, Osaka University,*
2–2 Yamadaoka, Suita, Osaka 565–0871, Japan

a) *yasuo_terasawa@nidek.co.jp*

Abstract: A visual prosthesis is an artificial sensory organ that transmits visual information to a blind person by electrically stimulating residual neurons in the visual nervous system. Such a system requires a large number of stimulating electrodes: It is technically difficult to connect a stimulator placed behind the ear to each of the stimulating electrodes over any significant distance with high reliability. We propose a visual prosthesis containing a multiplexer that is separately placed from the stimulator unit. The array of stimulating electrodes is connected to the stimulation unit through a multiplexer. The stimulating electrodes and multiplexer are placed onto the suprachoroidal space. The stimulation unit consists of a metal case and a coil and is implanted in the postauricular region of the cranium. The multiplexer and the stimulator unit are connected by a cable composed of six wires. Incorporating the multiplexer enables us to control of a large number of electrodes using a small number of conductors in the cable. We have developed a system with 100 electrodes which is powered and controlled wirelessly. Then we have confirmed that the proposed system functions successfully both in vitro and in vivo.

Keywords: visual prostheses, electrode, multiplexer
Classification: New functional devices and materials

References

[1] M. S. Humayun, J. D. Weiland, G. Y. Fujii, R. Greenberg, R. Williamson, J. Little, B. Mech, V. Cimmarusti, G. V. Boemel, G. Dagnelie, and E.

© IEICE 2008
DOI: 10.1587/elex.5.574
Received June 23, 2008
Accepted July 10, 2008
Published August 10, 2008

de Juan Jr, "Visual perception in a blind subject with a chronic microelectronic retinal prosthesis," *Vis. Res.*, vol. 43, pp. 2573–2581, 2003.

[2] E. Zrenner, A. Stett, S. Weiss, R. B. Aramant, E. Guenther, K. Kohler, K.-D. Milliczek, M. J. Seiler, and H. Haemmerle, "Can subretinal microphotodiodes successfully replace degenerated photoreceptors?," *Vis. Res.*, vol. 39, pp. 2555–2567, 1999.

[3] G. Richard, R. Hornig, M. Keseru, and M. Feucht, "Chronic Epiretinal Chip Implant in Blind Patients with Retinitis Pigmentosa: Long-Term Clinical Results," *Invest. Ophthalmol. Vis. Sci.*, vol. 48, no. 5, p. S666, 2007.

[4] H. Kanda, T. Morimoto, T. Fujikado, Y. Tano, Y. Fukuda, and H. Sawai, "Electrophysiological Studies of the Feasibility of Suprachoroidal-Transretinal Stimulation for Artificial Vision in Normal and RCS Rats," *Invest. Ophthalmol. Vis. Sci.*, vol. 45, no. 2, pp. 560–566, 2004.

[5] M. S. Humayun, J. Hopkins, S. H. Greenwald, A. Horsager, A. Roy, K. H. McClure, G. Palmer, I. Fine, M. J. McMahon, and R. J. Greenberg, "Electrical Effects and Perceptual Performance Using a Chronically Implanted 16–Channel Epiretinal Prosthesis in Blind Subjects," *Invest. Ophthalmol. Vis. Sci.*, vol. 47, no. 5, p. S3212, 2006.

[6] M. J. McMahon, A. Caspi, J. D. Dorn, K. H. McClure, M. S. Humayun, and R. J. Greenberg, "Spatial Vision in Blind Subjects Implanted With the Second Sight Retinal Prosthesis," *Invest. Ophthalmol. Vis. Sci.*, vol. 48, no. 5, p. S4443, 2007.

[7] G. Dagnelie, D. Barnett, M. S. Humayun, and R. W. Thompson, Jr, "Paragraph Text Reading Using a Pixelized Prosthetic Vision Simulator: Parameter Dependence and Task Learning in Free-Viewing Conditions," *Invest. Ophthalmol. Vis. Sci.*, vol. 47, no. 3, pp. 1241–1250, 2006.

[8] J. Sommerhalder, E. Oueghlani, M. Bagnoud, U. Leonards, A. B. Safran, and M. Pelizzone, "Simulation of artificial vision: I. Eccentric reading of isolated words, and perceptual learning," *Vis. Res.*, vol. 43, pp. 269–283, 2003.

[9] J. Ohta, T. Tokuda, K. Kagawa, T. Furumiya, A. Uehara, Y. Terasawa, M. Ozawa, T. Fujikado, and Y. Tano, "Silicon LSI-based smart stimulators for retinal prosthesis," *IEEE Eng. Med. Biol. Mag.*, vol. 25, no. 5, pp. 45–59, 2006.

[10] Y. Terasawa, H. Tashiro, A. Uehara, T. Saitoh, M. Ozawa, T. Tokuda, and J. Ohta, "The development of a multichannel electrode array for retinal prostheses," *J. Artif. Organs.*, vol. 9, pp. 263–266, 2006.

[11] T. Stieglitz, H. Beutel, R. Keller, C. Blau, and J.-U. Meyer, "Development of flexible stimulation devices for a retina Implant system," *Proceedings of the 19th Annual International Conference of the IEEE*, vol. 5, pp. 2307–2310, 1997.

[12] D. C. Rodger, W. Li, H. Ameri, S. Saati, P. Menon, E. Meng, J. D. Weiland, M. S. Humayun, and Y.-C. Tai, "Dual-Metal-Layer Parylene-Based Flexible Electrode Arrays for Intraocular Retinal Prostheses," *Invest. Ophthalmol. Vis. Sci.*, vol. 48, no. 5, p. S657, 2007.

[13] D. B. Shire, M. Gingerich, J. F. Rizzo, and J. L. Wyatt, "Recent Developments in Inflatable Prostheses for Epiretinal Stimulation and/or Recording," *Invest. Ophthalmol. Vis. Sci.*, vol. 46, no. 5, p. S1146, 2005.

© IEICE 2008
DOI: 10.1587/elex.5.574
Received June 23, 2008
Accepted July 10, 2008
Published August 10, 2008

ELectronics EXpress

IEICE Electronics Express, Vol.5, No.15, 574–580

1 Introduction

Recently, research both in Japan and overseas has accelerated in the field of artificial sight for patients with acquired sight disabilities; these efforts have concentrated on electrically stimulating the patient's remaining visual nervous system to transmit information to his visual center [1, 2, 3]. Our research group has been developing a system that uses suprachoroidal transretinal stimulation (STS) for this purpose [4]. Cochlear implants share many technical commonalities with visual prostheses, including signal transfer and wireless communication. One research group is actually pursuing development of an artificial vision system in collaboration with a cochlear implant manufacturer [1, 5, 6]. However, there is the technical challenge of establishing an electric connection over the considerable distance from the interiors of the eyeballs to the stimulator unit implanted behind the ears without any cable interruptions due to eye movement. The larger the number of electrodes, the more difficult this becomes. Simulations of artificial vision systems have suggested that over 100 electrodes are necessary to permit activities of daily living (ADL) such as face recognition and walking [7, 8]. One procedure that has been proposed to solve this problem involves combining the stimulating electrode and a miniaturized electronic circuit into a single unit [9]. Another method is to use a multiplexer; this would allow a low number of wires to be used until just before connecting to the stimulating electrodes.

This report proposes an artificial sight system that includes the best features of the cochlear implant, but incorporates a multiplexer that is separate from the hermetically sealed stimulation unit, thus permitting a large number of stimulating electrodes to be used. An implantable wireless power supply and transmitting device were also constructed. Validation tests results and

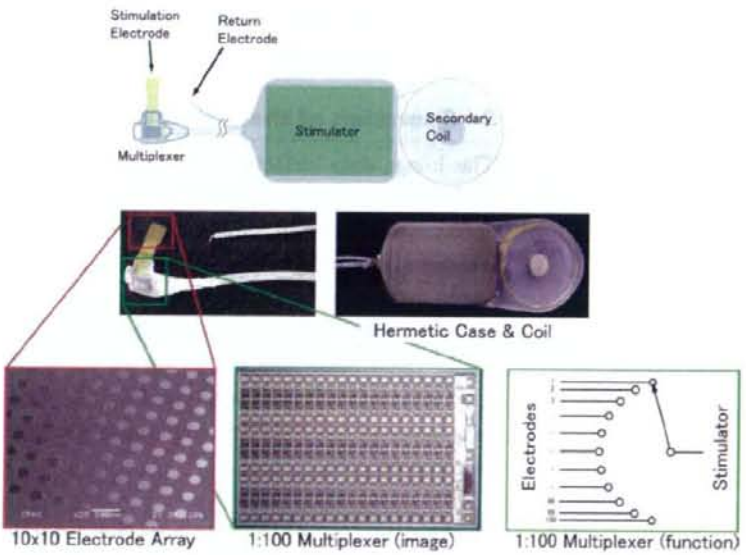

Fig. 1. overview of retina prosthesis.

© IEICE 2008
DOI: 10.1587/elex.5.574
Received June 23, 2008
Accepted July 10, 2008
Published August 10, 2008

ELectronics EXpress

IEICE Electronics Express, Vol.5, No.15, 574–580

directions for future research efforts are discussed.

2 Design of a retinal prosthesis with 100 stimulation electrodes

An artificial vision system consists of both implanted and external components. Figure 1 shows a diagram of the implanted device; it consists of a secondary coil, a stimulator in a hermetically sealed case, a multiplexer, and stimulating and return electrodes. Just as in a cochlear implant, the stimulation unit is implanted behind the ear. The stimulating electrodes and multiplexer are placed on the sclera. The stimulator and multiplexer are connected via a cable composed of six wires which provide power for the multiplexer, the selection signal for the electrode, and the stimulator pulses. Each of the conductors is a stainless steel seven-stranded wire covered with a Teflon insulator. The six conductors and each stimulating electrode are connected with the input/output pads of the multiplexer. A custom integrated circuit (IC) was designed as a multiplexer and is mounted in a flip chip format directly on the board for the stimulating electrodes, with gold bump connections. This chip has dimensions of $4.9 \times 3.2 \times 0.57$ mm (thickness) and was manufactured in a 2 poly-2 metal high-voltage complementary metal oxide semiconductor (CMOS) process. Except for the stimulating electrodes and cables, the entire device is double-coated with $1\,\mu$m of parylene N and $5\,\mu$m of parylene C. The multiplexer is also then coated with silicone molded into a curve that fits the eyeball.

The stimulating electrodes consist of one layer each of gold and platinum on a polyimide base in the form of a 10×10 array of bumps, $200\,\mu$m in diameter, and $30\,\mu$m high. The outermost face of the array is coated with parylene C with just the tips of bumps exposed. More complete details about the electrodes are presented in a previous report [10]. The stimulation unit case is made of titanium hermetically sealed by electron beam welding.

3 Operation of the retinal prosthesis

The image data detected by the camera and transmitted to the external device is transferred along with power to the implanted device. Wireless transmission is on an amplitude-modulated carrier frequency of 16.64 MHz. The internal voltage of the implant is monitored regularly by back-telemetry of the load modulation. Stimulating current pulses are generated using the signals detected by the implanted device and transmitted via the multiplexer to the electrodes. The source circuit can apply a maximum of 10 V to the load. On the basis of instructions from the implanted device, the multiplexer selects one of the 100 electrodes and connects it to the current source in the stimulation unit.

4 Experimental results and discussion

First, in order to verify that the current required by the external device was being output from the designated electrode, a probe was directly attached

© IEICE 2008
DOI: 10.1587/elex.5.574
Received June 23, 2008
Accepted July 10, 2008
Published August 10, 2008

to each stimulating electrode. The probing was performed automatically by controlling the position of the XYZ stage. Normal operation and wire connection of the implant such as electrode selection and controlling of the pulse parameters were confirmed with the use of the probing system. Cracks appeared on the surfaces of some electrodes where the probes came into contact with them. Future research is required to determine whether this can be solved by using a softer material for the probes, or by incorporating a liquid conductor.

An operation test was performed under phosphate-buffered saline (PBS). Figure 2 shows a photograph of the experimental setup. Three devices were submerged in 23°C PBS and supplied with a pulsed current for 72 hours. The pulse parameters were cathodic-first, 100 μs-duration, symmetric biphasic, 600 μA-amplitude at 100 Hz. The changes in the output current in response to changes in the image captured by a camera were monitored using an oscilloscope and a current probe (Fig. 2). Two of the three devices tested showed the expected response within the time tolerance. The other did not appear to be functioning properly, since some stimuli were delivered properly, while others were not delivered at all. It is quite likely that there were faulty connections at the multiplexer. Improving the reliability of these connections needs to be addressed in future research.

Finally, the functioning of implanted devices in vivo was checked. The left side of Fig. 3 shows a photograph of the experimental system. The internal device was implanted inside the subcutaneous pocket in the rabbit's back. Wireless power transmission was regularly conducted from the external device to the internal device starting before the procedure and continuing 7 days after the procedure. The internal voltage in the device was then verified by back telemetry. Figure 3 shows the time-dependent changes in the internal voltage of the implanted device. The voltage remained at the specified level until the 10th day after implantation, implying that the device was operating normally. All of the records for this in vivo experiment were maintained in compliance with the ARVO statement.

In this study, we employed a multiplexer to connect the many electrodes.

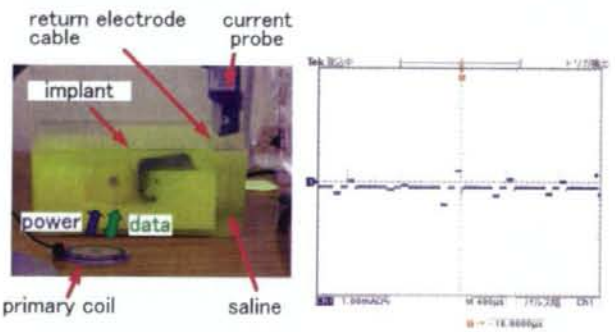

Fig. 2. Experimental setup (left) and current waveforms (right).

© IEICE 2008
DOI: 10.1587/elex.5.574
Received June 23, 2008
Accepted July 10, 2008
Published August 10, 2008

ELectronics EXpress

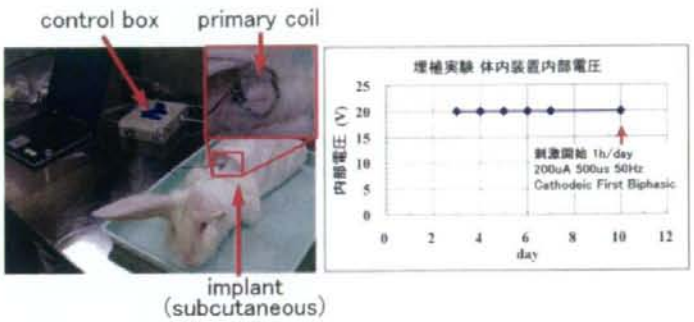

Fig. 3. Experimental setup (left) and current waveforms (right).

If the micro wiring that has been developed along with other dramatic advances in semiconductor manufacturing technologies is used for these connections, it will no longer be very difficult to provide large numbers of conductors in small spaces. Steiglitz et al. succeeded in placing 25 platinum conductors on a 1.2-mm-wide polyimide strap [11], and further miniaturization of conductors is possible. It has been shown to be possible to place small conductors on a parylene substrate [12, 13]. However, these schemes rely on thin films of noble metals, and would have high resistance due to the small conductor area. For example, a platinum film conductor that is 20 μm wide, 0.1-μm thick and 200 mm long, would have an estimated resistance of 10.6 kΩ. This impedance is approximately equal to that of typical biological tissue. The wiring resistance would require high source voltages in order to drive the circuit and would increase the power consumption. The volume resistivity of thin film conductors is known to be higher than that of bulk conductors, and the actual resistance would be even higher than the estimate given above. Wires of larger cross-sectional area could be used to avoid this. If they were used, however, a bundle of 100 such wires would be stiff, heavy, and thick, and so would be problematic for actual implants. Therefore, in order to create systems resembling the cochlear implant with many electrodes, we believe that the most practical approach is the multiplexer-based system proposed here.

Except for the multiplexer, the circuits for the device manufactured for this study were placed inside a hermetically sealed package. The multiplexer was covered with parylene and silicone, but it would be preferable to also install the multiplexer in a hermetically sealed container in order to ensure long-term reliability. However, it is technically difficult to create small sealed packaging for something as small as this component which is to fit against the client's eye. This advance is left to future research.

5 Conclusions

We have proposed architecture for an artificial vision system containing 100 electrodes for stimulating the optic nerve. We have succeeded in creating a

© IEICE 2008
DOI: 10.1587/elex.5.574
Received June 23, 2008
Accepted July 10, 2008
Published August 10, 2008

wireless system for transmission of power and communications. The devices continued to function normally while submerged in a normal saline solution and while implanted for extended periods of time. Future research will address increasing the number of electrodes and developing a hermetically sealed version of the multiplexer.

© IEICE 2008
DOI: 10.1587/elex.5.574
Received June 23, 2008
Accepted July 10, 2008
Published August 10, 2008

Direct Effect of Electrical Stimulation on Induction of Brain-Derived Neurotrophic Factor from Cultured Retinal Müller Cells

Tatsuhiko Sato,[1] Takashi Fujikado,[1] Tong-Sheng Lee,[1] and Yasuo Tano[2]

Purpose. To investigate the direct effect of electrical stimulation (ES) on the induction of brain-derived neurotrophic factor (BDNF) from cultured retinal Müller cells.

Methods. Müller cells were isolated from rat retinas. ES was applied to passage 1 Müller cells with biphasic pulses (duration, 1 ms; frequency, 20 Hz; current, 10 mA) for 30 minutes. The changes in gene expression after ES were analyzed with microarrays. The mRNA and protein levels of BDNF were determined at each time point after ES by RT-PCR and ELISA, respectively. RT-PCR was also performed at 3 hours after ES of Müller cells that had been exposed to 1 μM nifedipine, a blocker of L-type voltage-dependent calcium channels (L-VDCCs).

Results. Microarray analyses showed an upregulation of 245 genes, including BDNF. The mRNA level of BDNF increased significantly ($P < 0.05$; by ~1.2-fold over that of the control) at 2 and 3 hours after ES. The intracellular protein level was upregulated significantly (by ~1.4-fold) at 6 hours after ES, whereas the extracellular level did not change at any time point. The total protein level of BDNF increased significantly (~1.3-fold) at 6 hours after ES. The increase in the mRNA level of BDNF was fully suppressed by exposure of the Müller cells to nifedipine.

Conclusions. These results demonstrate that ES directly upregulates the transcriptional induction of BDNF through L-VDCCs in cultured Müller cells. The ES of Müller cells may be used to supply endogenous BDNF to the retina. (*Invest Ophthalmol Vis Sci.* 2008;49:4641–4646) DOI:10.1167/iovs.08-2049

Müller cells, the predominant glial element in the retina, are believed to play important roles in maintaining its integrity and function. For example, Müller cells have been shown to express glutamate transporters,[1] which are postulated to contribute to the clearance of glutamate and protect retinal ganglion cells (RGCs) from glutamate neurotoxicity.[2–5] Müller cells also synthesize glutamine synthetase[6] which amidates glutamate to form the non-neuroactive compound glutamine.[7] In addition, Müller cells produce various neurotrophic factors, including brain-derived neurotrophic factor (BDNF),[8,9] basic fibroblast growth factor (bFGF or FGF-2),[10,11] and insulin-like growth factor (IGF)-1,[12] in reaction to different in vivo and in vitro conditions.

We have demonstrated that electrical stimulation (ES) induces the transcription of IGF-1 from cultured Müller cells and that the induction was dependent on calcium (Ca^{2+}) influx through L-type voltage-dependent calcium channels (L-VDCCs).[13] Ca^{2+} ions are the most widely used second messengers, and many of the processes that occur in the central nervous system (CNS; e.g., gene transcription), are controlled by Ca^{2+} influx.[14] For example, Ou and Gean[15] showed that the Ca^{2+} influx through *N*-methyl-D-aspartate (NMDA) receptors and L-VDCCs upregulated the transcription of BDNF in the amygdala. Sasaki et al.[16] demonstrated that Ca^{2+} entry into cortical neurons through L-VDCCs induced neuronal nitric oxide synthase (nNOS) message as well as protein synthesis. On the other hand, ES has been reported to induce different gene expressions (e.g., BDNF,[17,18] bFGF,[18] and growth-associated protein [GAP]-43[19] in both central and peripheral neurons. In addition, ES has been demonstrated to induce expression of various genes by Ca^{2+} influx through VDCCs in neurons other than those of the retina.[20,21]

Thus, we hypothesized that the Ca^{2+} influx into Müller cells via L-VDCCs that is induced by ES increases the gene expression of neurotrophic factors. To test this hypothesis, we initially performed microarray analyses to evaluate the changes in gene expression with and without ES in cultured Müller cells. Our results showed that the mRNA of BDNF was upregulated, and the time course of BDNF expression at both the message and protein levels was determined.

Materials and Methods

All experimental procedures were performed in accordance with the ARVO Statement for the Use of Animals in Ophthalmic and Vision Research and were approved by the Animal Research Committee, Osaka University Medical School.

Müller Cell Cultures

Müller cells were obtained by a method that isolates cells that were >95% pure Müller cells.[15,22] Briefly, eye cups from Long-Evans rats at postnatal days 12 to 14 were soaked in Dulbecco's modified Eagle's medium (DMEM; Nikken Biomedical Laboratory, Kyoto, Japan) supplemented with 1:1000 penicillin/streptomycin (Invitrogen Japan, Tokyo, Japan) overnight at room temperature in the dark. The eye cups were then incubated in DMEM containing 0.05% trypsin/EDTA (Invitrogen Japan) and 70 U/mL collagenase (Sigma-Aldrich, Tokyo, Japan) for 30 minutes at 37°C. The retinas were dissociated into small aggregates with a narrow-bore Pasteur pipette in culture medium. The culture medium was low-glucose DMEM supplemented with 10% fetal bovine serum (Invitrogen Japan) and 1:1000 penicillin-streptomycin. The cells were seeded into culture dishes and maintained at 37°C in a humidified atmosphere of 5% CO_2 and 95% air. When the primary cells proliferated to 80% to 90% confluence, the cells were passaged with Dulbecco's phosphate-buffered saline (DPBS; Nikken Biomedical Laboratory) supplemented with 0.05% trypsin/EDTA. The cells were seeded at the same concentration into 35-mm dishes in 2 mL fresh culture medium.

From the Departments of [1]Applied Visual Science and [2]Ophthalmology, Osaka University Medical School, Osaka, Japan.

Supported by Health Sciences Research Grant H16-sensory-001 from the Ministry of Health, Labor, and Welfare, Japan, and by Grant 18591918 from the Ministry of Education, Culture, Science, and Technology.

Submitted for publication March 19, 2008; revised April 23 and May 20, 2008; accepted August 8, 2008.

Disclosure: **T. Sato**, None; **T. Fujikado**, None; **T.-S. Lee**, None; **Y. Tano**, None

The publication costs of this article were defrayed in part by page charge payment. This article must therefore be marked "*advertisement*" in accordance with 18 U.S.C. §1734 solely to indicate this fact.

Corresponding author: Takashi Fujikado, Department of Applied Visual Science, Osaka University Medical School, 2-2 Yamadaoka, Suita, Osaka 565-0871, Japan; fujikado@ophthal.med.osaka-u.ac.jp.

Copyright © Association for Research in Vision and Ophthalmology

Cells of passage 1, which were cultured strictly for the same period to subconfluent condition, were used in all experiments for the statistical analyses.

Conditions of ES

ES was applied to Müller cells on a clean bench.[13] Briefly, silver/silver chloride needle-type electrodes (ϕ = 0.2 mm) were inserted into culture medium without touching the Müller cells. The distance between the two electrodes was 20 mm. A rectangular biphasic train of pulses (pulse duration, 1 ms; pulse frequency, 20 Hz; current intensity, 10 mA) was delivered between the electrodes continuously for 30 minutes through a stimulus isolation unit for delivery of a constant current (Stimulator SEN-7203; Nihon Kohden, Tokyo, Japan; Isolator A395R; World Precision Instruments, Sarasota, FL), as in our previous study.[13] The voltage between the electrodes was monitored on a 40-MHz oscilloscope (CS-4135A; Kenwood, Tokyo, Japan).

In control experiments, cells without ES were maintained on the bench for 30 minutes.

Microarray Analyses

To minimize the variations among the cell samples, the Müller cells from three dishes with or without ES were combined as the ES or control groups, respectively. Total RNA was isolated immediately after ES with an extraction reagent (RNeasy Mini Kit; Qiagen Japan, Tokyo, Japan) according to the manufacturer's protocols. The RNA samples were hybridized to a rat array containing 31,099 target probe sets (GeneChip Rat Genome 230 2.0 Array; Affymetrix Japan, Tokyo, Japan) and the following experiments were performed according to the manufacturer's recommendations.

The signal intensities were calculated with the microarray software (GeneChip Operating Software; Affymetrix Japan). If the raw signal intensities were <0.01, they were set to 0.01 according to the manufacturer's protocols. The raw intensity values in each chip were normalized to the 50th percentile of the measurements. Each gene was normalized to the median of that gene in the respective ES or control groups. Further analyses were performed with a second software program (GeneSpring 7.2 software; Agilent Technologies Japan, Tokyo, Japan) to compare the transcriptional inductions in the ES group with the control.

Quantitative Real-Time PCR

The mRNA levels of BDNF were determined by quantitative real-time PCR (RT-PCR) at 0, 1, 2, 3, and 6 hours after ES and calculated by the comparative C_t method.[23] β-Actin was used as the endogenous control. Total RNA was isolated by the method just described and was reverse transcribed to synthesize cDNA (First-Strand cDNA Synthesis System for Quantitative RT-PCR; Marligen Bioscience, Ijamsville, MD). RT-PCR was then performed (Prism 7900HT; Applied Biosystems [ABI] Japan, Tokyo, Japan) in a 384-well format by selecting primer and probe sets (*Taq*Man) from an online catalog (BDNF: *Taq*Man [ABI] Gene Expression Assay ID, Rn02531967_s1, Celera Annotation GenBank accession No. NM_178866.2; β-actin: ID Rn00667869_ml, No. NM_031144.2; http://www.ncbi.nlm.nih.gov/Genbank; provided in the public domain by the National Center for Biotechnology Information, Bethesda, MD). The sequences of the primers and probes are not disclosed. The thermal cycling conditions were: 50°C for 2 minutes, 95°C for 10 minutes, and 40 cycles at 95°C for 15 seconds and 60°C for 1 minute. Each measurement was performed in duplicate in six independent runs.

The expression of BDNF gene in the ES group was compared to that in the control group. The relative data are presented as the mean multiple of change (*x*-fold) ± SD calculated from the six separate experiments. The Wilcoxon signed rank test was used to analyze the statistical significance ($P < 0.05$) of differences between the median values.

Enzyme-Linked Immunosorbent Assay

Both extracellular and intracellular BDNF protein levels were measured at 3, 6, 12, 24, and 48 hours after ES by quantitative sandwich enzyme immunoassay (Chemicon International, Temecula CA) according to the manufacturer's instructions. This technique can measure both human and rat BDNF. The culture medium and the cell lysate were collected as the samples for extracellular and intracellular BDNF, respectively. To lyse the Müller cells, the cells were soaked in 200 μL of lysis buffer (RIPA buffer; Sigma-Aldrich) supplemented with a protease inhibitor cocktail (Protease Inhibitors Mixture for Protease and Esterase; Wako, Osaka, Japan). The lysate was centrifuged at 15,000 rpm for 10 minutes at 4°C, and the BDNF in the supernatant was measured as intracellular BDNF.

The optical density of each sample was measured at 450 nm with the correction wavelength set at 540 nm ($ARVO_{MX}$; PerkinElmer Japan, Kanagawa, Japan). Each measurement was performed in duplicate in six independent runs. The absolute protein amount of BDNF was calculated by the following equations:

$$\text{Extracellular BDNF (pg)} = \text{medium concentration (pg/mL)} \times 2 \text{ (mL, medium volume)},$$

$$\text{Intracellular BDNF (pg)} = \text{lysate concentration (pg/mL)} \times 0.2 \text{ (mL, lysate volume)},$$

and

$$\text{Total BDNF (pg)} = \text{sum of extra- and intracellular BDNF (pg)}.$$

The expression of the protein BDNF in the ES group was compared with that in the control group. The relative data are presented as the mean multiple of change ± SD calculated from six separate experiments. The Wilcoxon signed rank test was used to analyze the statistical significance ($P < 0.05$) of differences between the medians.

Quantitative Real-Time PCR with L-VDCC Blocker

The mRNA level of BDNF in Müller cells exposed to 1 μM nifedipine was determined by RT-PCR at 3 hours after ES and compared with that in Müller cells without nifedipine. Briefly, 1 μM nifedipine was added to the culture medium immediately before the start of ES. The dose of nifedipine was enough to block the Ca^{2+} influx via L-VDCCs.[13] ES was applied to Müller cells, and thereafter the medium of the dishes with and without ES was replaced by 2 mL fresh culture medium.

The mRNA level of BDNF in Müller cells without ES and nifedipine was normalized to 1, and the relative data are presented as the mean multiple of change ± SD calculated from twelve separate experiments. The Kruskal-Wallis one-way ANOVA on ranks was used to analyze the statistical significance ($P < 0.05$) of the differences among the median values, followed by Dunn's method to determine significant differences between each group.

Results

These experiments were conducted on passage 1 Müller cells because the primary-culture cells were contaminated by many other cell types, and preliminary assays by RT-PCR showed marked variations in the expression levels of several genes among the culture dishes (data not shown). Examination of the cells with an optical microscope showed that the morphologic appearance of the Müller cells did not change after the different experimental procedures.

Microarray Analyses

In our earlier study,[13] a Ca^{2+} influx into Müller cells was detected immediately after the beginning of ES, and the mRNA of IGF-1 was upregulated at the cessation of ES. Thus, to evaluate the direct effect of ES on the changes in gene expression, we performed microarray analyses on cells isolated immediately after ES.

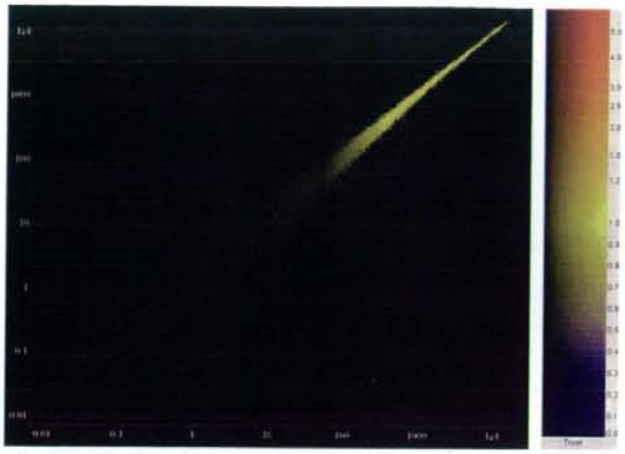

A

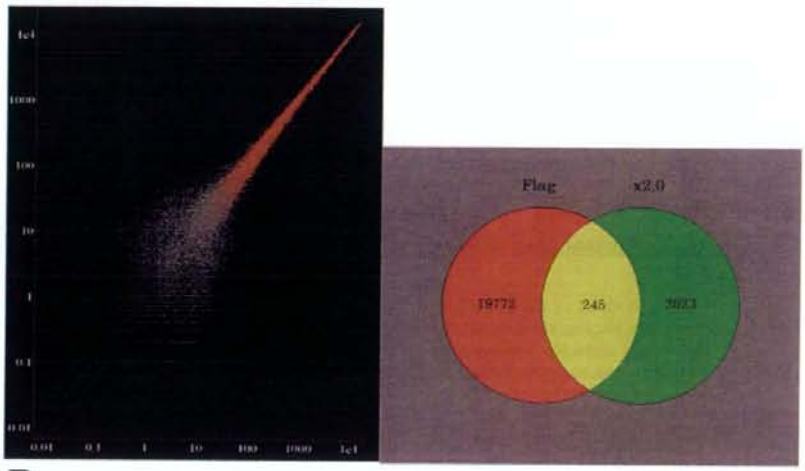

B

FIGURE 1. Results of microarray analyses. The horizontal and vertical axes represent the signal intensity of the genes expressed in the control and ES groups, respectively. (**A**) Signal intensity image plot of all gene expressions (31,099 probes). For each probe, the ratio of the signal intensity in the ES group to that in control is represented by a color, according to the vertical strip. (**B**) The circle of Flag contains the genes with signals that were "present" or "marginal" in the ES or control groups or both. The circle of ×2.0 holds the genes showing a more than twofold signal intensity in ES compared with the control. *Left*: signal intensity image of the probes, which corresponds to the pie chart.

The results showed that 7.3% (2268) of the probes expressed more than a twofold higher signal intensity in the ES group than in the control (Fig. 1A). The probes whose signals were absent in both the ES and control groups were not analyzed, according to the manufacturer's recommendations. The number of probes showing sufficient intensities that were more than two times higher in the ES than in the control was 245 (Fig. 1B). The genes associated with nervous system development were selected and are listed in Table 1. The most well-known neurotrophic factor was BDNF, with a gene expression that changed from absent in the control to a 2.6-fold increase in the ES group. Thus, the following experiments were focused on BDNF.

TABLE 1. Results of Microarray Analyses Immediately after ES

Description	GenBank Accession No.	Normalized Signal Intensity in Control	Flags of Control	Normalized Signal Intensity in ES	Flags of ES
Dihydropyrimidinase-like 3	AI059953	1.00	A	2.02	P
Zinc finger and BTB domain containing 16	BG371725	1.00	A	2.15	P
Ectodermal-neural cortex 1	AA997271	1.00	M	2.19	A
Brain derived neurotrophic factor	X67108	1.00	A	2.58	P
Stathmin-like 3	NM_024346	1.00	A	3.31	M
UDP galactosyltransferase 8	L21698	1.00	A	13.77	P

A, absent; M, marginal; P, present.